# A near-infrared carbon dioxide sensor system using a compact folded optical alignment structure

Zhiwei Liu[ad], Chuantao Zheng[*ad], Hongtao Xie[ad], Qiang Ren[b], Chen Chen[b], Weilin Ye[*c], Yiding Wang[ad] and Frank K. Tittel[e]

[a]State Key Laboratory of Integrated Optoelectronics, College of Electronic Science and Engineering, Jilin University, 2699 Qianjin Street, Changchun, 130012, P.R. China ; [b]College of Instrumentation & Electrical Engineering, Jilin University, 938 Ximinzhu Street, Changchun, 130021, P.R. China; [c]College of Engineering, Shantou University, 243 Daxue Road, Shantou 515063, China; [d]Jilin Provincial Engineering Research Center of Infrared Gas Sensing Technique, 2699 Qianjin Street, Changchun 130012, China; [e]Department of Electrical and Computer Engineering, Rice University, 6100 Main Street, Houston, TX 77005, USA

## ABSTRACT

A compact optical alignment structure and a novel beam-tracing method were proposed for tunable laser absorption spectroscopy (TLAS) based gas measurements, in order to minimize sensor size and ease beam alignment procedure. A near-infrared carbon dioxide ($CO_2$) sensor system was developed based on the alignment structure. A distributed feedback (DFB) laser centered at 6361.3 $cm^{-1}$ and a multi-pass gas cell (MPGC) with an effective optical path length of 29.8 m were employed. The sensor system was integrated as standalone equipment by customizing an aluminum baseplate for a stable field operation. A series of experiments were carried out to assess the performance of the sensor system. A limit of detection (LoD) of ~ 7.1 parts-per-million in volume (ppmv) at a 0.4 s averaging time was obtained, and the LoD was reduced to ~ 277 parts-per-billion in volume (ppbv) at an optimum averaging time of 153.6 s. Considering gas mixing times, the rise and fall time were measured to be ~ 290 s and ~ 200 s, respectively.

**Keywords:** laser absorption spectroscopy, infrared absorption, natural gas hydrates, carbon dioxide sensor

## 1. INTRODUCTION

Natural gas hydrates, regarded as a new type of energy material with great application potentials in the 21th century, have been explored on the worldwide seafloor[1, 2]. In recent years, two methods, including marine deep-tow seismic technique[3] and spectroscopy-based geochemical detection[4] were employed to measure gas species escaping from the seabed for the content analysis of natural gas hydrates. However, these reported techniques cannot achieve both high accuracy and in situ measurement as required. In addition, the existing techniques usually need large-size and complicated facilities, increasing the difficulty in gas detection under water. An infrared laser absorption spectroscopy (LAS) based gas sensing method[5] is widely used in atmospheric and environmental monitoring, which has a high accuracy up to the level of parts-per-billion by volume (ppbv) and a non-contact *in situ* detection performance. A compact LAS sensor system aiming at new resource exploration is required for the detection of the gas species from a deep-sea gas-liquid separator using this technique.

Tunable laser absorption spectroscopy (TLAS) in the infrared band[6-8] was widely used for trace gas detection and has been applied in sensitive gas measurements in a variety of fields, such as, in environmental monitoring[9-11] and industrial applications[12-13]. A TLAS based gas sensor system[14, 15] consists of a light source targeting an absorption line of a specific gas, a gas cell for the interaction between gas molecule and infrared light, and a detector for the transformation from a lightwave to an electrical signal. Optimum beam alignment structure related to these three components is important for improving sensor performance. Furthermore sensor size and design complexity are other factors that are important in establishing the optical path. A near-infrared source produces a laser beam via a pigtail fiber, which can be connected directly to a cell through a fiber connector. However, for a mid-infrared laser, optical components and a

*zhengchuantao@jlu.edu.cn; wlye@stu.edu.cn; phone 13756090979;

Advanced Sensor Systems and Applications VIII, edited by Tiegen Liu, Shibin Jiang, Proc. of SPIE
Vol. 10821, 108210I · © 2018 SPIE · CCC code: 0277-786X/18/$18 · doi: 10.1117/12.2502445

proper alignment method are required. Generally, the reported optical structure[16-18] used a dichroic mirror to combine the invisible infrared light with a visible laser beam for alignment.

In order to minimize sensor size and facilitate the beam alignment procedure (required for some special application, e.g. deep-sea gas measurement), a more simple and compact optical structure for TLAS-based *in situ* gas detection was proposed and functionally verified. In comparison with the reported structure in[16], the dichroic mirror and the focusing lens were removed in order to reduce the sensor size and a new near-infrared $CO_2$ sensor system was developed. A distributed feedback (DFB) laser centered at 6361.3 $cm^{-1}$ and a multi-pass gas cell (MPGC)[19] with an effective optical path length of 29.8 m were employed. Moreover, the sensor system was integrated as a standalone equipment by adopting a custom aluminum baseplate for a convenient deployment and stable operation of the sensor. A series of experiments were carried out to assess the performance of the sensor system, which provides the basis for the further development of a mid-infrared $CO_2$ sensor system with a limit of detection (LoD) of ppbv via the use of a mid-infrared tunable laser.

## 2. $CO_2$ SENSOR SYSTEM CONFIGURATION

### 2.1 Folded optical alignment structure

In order to enhance the mechanical stability, an aluminum plate was used to mount the optical sub-system, which consists of a light source, a gas cell, a photoelectric detector and three reflectors. The MPGC, with a special dense spot pattern, provides a sealed environment for the interaction between gas molecules and the infrared light. The cell offers a 29.8 m effective optical path length after 215 reflections with a physical size of 20×16×5 $cm^3$. A near-infrared DFB laser was used as the optical source and two three-dimensionally adjustable mirrors (M1 and M2) were employed to guide the infrared beam into the MPGC. The output beam was focused onto an In-Ga-As (IGA) detector (Thorlabs, model PDA10D-EC) using a parabolic mirror (PM, $d$ = 25.4 mm, $f$ = 50.8 mm).

A 635 nm visible laser was used for beam alignment and a novel beam-tracing method was employed. Fig. 1 shows the optical alignment structure and the red and gray lines represent the infrared and visible beam, respectively. The MPGC, which is regarded to be the key unit of the optical sub-system, was initially fixed on an aluminum baseplate. The visible light from the alignment laser entered the MPGC according to a specific position and angle to obtain a mode pattern shown in the inset by carefully adjusting M2 and the output beam was focused on the IGA by the PM. Once a correct light path was achieved based on the visible beam, the next step is to align the infrared beam with the visible beam. For this purpose, the mirror M1 was installed on a 90° flip mount (Thorlabs, model FM90/M), which can repetitively switch the incident beam between the alignment laser and the DFB laser. Plane mirror (M3) was placed between M1 and M2 to reflect the incident beam to the direction opposite to the optical sub-system for alignment observation. Along the reflected optical path by M3, two stably-fixed paperboards were used to mark the spot positions (S1, S2) by painting two dots which can be considered as a description of the light path of the visible beam. After the marking process of the visible beam path, the DFB laser was powered on and a thermo-sensitive laser viewing card was used to observe the spot of the infrared light. In this procedure, the position and reflection angle of M1 were carefully adjusted to make sure that the infrared spots on M1, M3, S1 and S2 coincide with the visible spots, respectively. By adjusting M1, the spot positions of these two beams can be observed with high accuracy. A simultaneous monitor on the IGA output and a slight adjustment of M1 are also needed to obtain a final optical path as described by the red lines in Fig. 1.

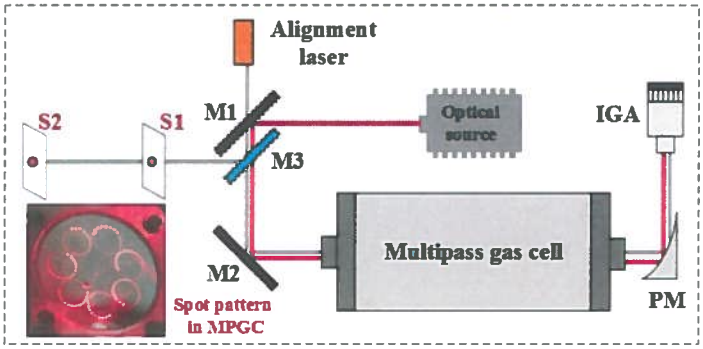


Figure 1. Diagram of the optical path alignment process employing a novel beam-tracing method.

## 2.2 Sensor design

A wavelength modulation spectroscopy (WMS)[20-22] based $CO_2$ sensor system was developed based on the compact folded optical structure. As depicted in Fig. 2(a), the system consists of an electrical and an optical sub-system. In the electrical part, a laser drive module (Wavelength Electronics, model LDTC0520) including a temperature controller and a current driver were employed for stabilizing the laser temperature and supplying a laser current. A dual-channel lock-in module was used to generate a saw-tooth scan signal superimposed by a sinusoid modulation signal for the current driver and also to extract the 2*f* signal from the IGA output signal. Another saw-tooth signal synchronized with the scan signal generated by the lock-in module was converted to a square-wave signal in order to trigger data sampling. A digital signal processor (DSP, Texas Instruments, model TMS320F28335) based data acquisition module was used for 2*f* signal acquisition. The DSP also delivered the 2*f* signal, 2*f*-amplitude and concentration to a laptop for data-record and post analysis. Furthermore, a compact power supply module with a direct current supply voltage of 24 V was developed for the whole sensor system. Fig. 2(b) shows the assembled equipment with a physical size of 52×30×27 $cm^3$ including the optical sub-system on the baseplate and the electrical sub-system. Fig. 2(c) is the top view of the optical path structure described in Sect. 2.1.

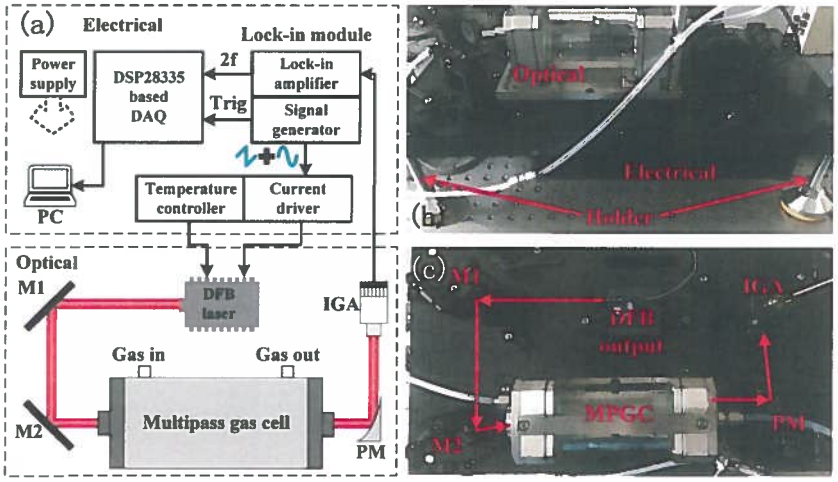


Figure 2. (a) Schematic of the $CO_2$ sensor system including an electrical and an optical sub-system. DFB: distributed feedback; IGA: InGaAs detector; M: plane mirror; PM: parabolic mirror. (b)Photograph of the integrated sensor system. (c) Top view of the optical structure.

## 2.3 Modulation depth optimization of the laser

For $CO_2$ concentration measurement, the 6359.96 $cm^{-1}$ absorption line[23, 24] was selected and a near-infrared DFB laser centered at 6361.3 $cm^{-1}$ was used as the light source. To obtain the optimum sensing performance, a gas mixing system (Environics, series 4000) was used to generate a $CO_2$ sample of 4000 parts-per-million by volume (ppmv) by diluting a standard 1% $CO_2$ with pure nitrogen ($N_2$) for modulation depth optimization of the laser. The experiment was conducted at a pressure of 1 atm. By applying a sinusoidal modulation signal of 5 kHz with different modulation amplitudes, the obtained 2*f* signal and its amplitude were recorded. The maximum 2*f* signal amplitude was achieved when the modulation depth was 0.31 $cm^{-1}$, corresponding to a modulation amplitude of 0.45 V, as depicted in Fig. 3.

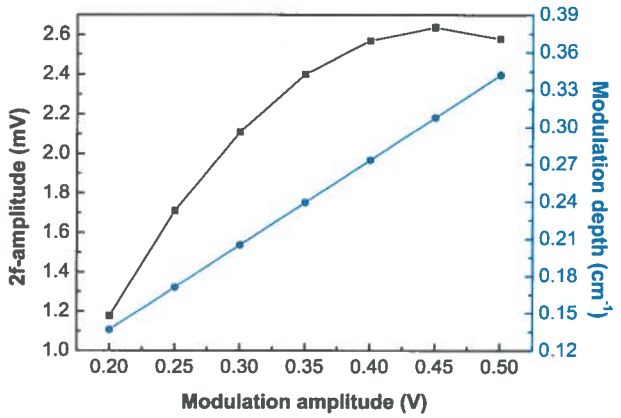


Figure 3. The 2*f* signal amplitude and modulation depth as a function of the modulation amplitude for a 4000 ppmv $CO_2$ sample.

## 3. EXPERIMENT AND RESULTS

### 3.1 Sensor calibration

A saw-tooth signal with a voltage range of 2 – 3.8 V and a frequency of 10 Hz superimposed by a 5 kHz sinusoidal modulation signal with an amplitude of 0.45 V was applied on the DFB laser. A gas mixing system was used to generate six $CO_2$ samples with a concentration range of 0 – 5000 ppmv. At each concentration level, the measured 2*f* signal amplitude were recorded for 5 minutes' intervals, as shown in Fig. 4(a). Then, the 2*f*-amplitude of each concentration were averaged and plotted as a function of the theoretical concentration value. As depicted in Fig. 4(b), by a linear data-fitting, an equation between the 2*f*-amplitude (i.e. max(2*f*)) and the gas concentration (*C*) was obtained

$$C = 1520.41196 \max(2f) - 14.03115 \quad (1)$$

Using the measured 2*f*-amplitude, the $CO_2$ concentration can be determined based on Eq. (1).

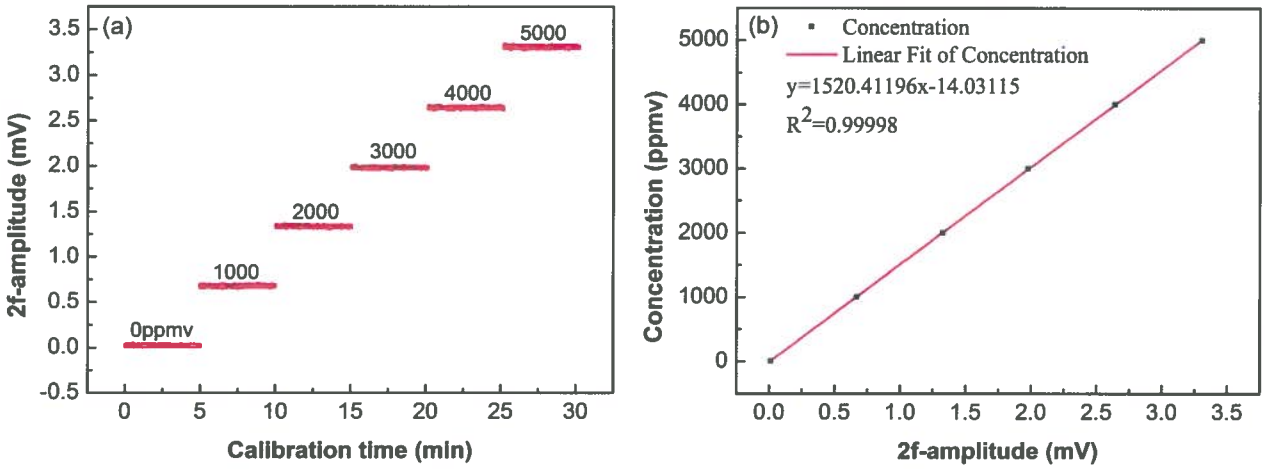


Figure 4. (a) Measured curves of the 2*f*-amplitudes versus calibration time for the 0, 1000, 2000, 3000, 4000, 5000 ppmv $CO_2$ samples. (b) Measured data dots and fitting curve of the $CO_2$ concentration versus 2*f*-amplitude.

### 3.2 Stability

The stability of the sensor system was tested by injecting N2 into the MPGC to eliminate the influence of the fluctuation of the gas concentration brought by the gas mixing system. An experiment lasting ~ 30 min was performed and the measured $CO_2$ concentration with a data sampling period of 0.4 s was recorded. An Allan deviation analysis was

employed to characterize the stability and the limit of detection (LoD). Fig. 5 exhibits the time series of the measured concentration levels and the Allan deviation versus the averaging time $\tau$. An LoD of ~ 7.1 ppmv for a 0.4 s averaging time was achieved and an optimum averaging time of 153.6 s corresponding to a LoD of ~ 277 ppbv was observed. The red line proportional to 1/sqrt($\tau$) expresses the theoretical performance of a system impacted by White-Gaussian noise only.

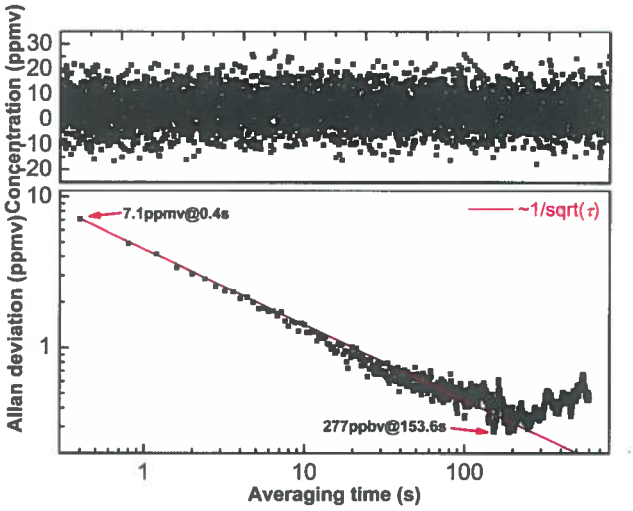


Figure 5. Measured concentration of a 0 ppmv $CO_2$ sample and the Allan deviation analysis of the sensor system.

### 3.3 Response time

A continuous dynamic measurement was performed for ~ 25 min to determine the response behavior of the sensor system. The gas mixing system was used to produce three $CO_2$ samples whose concentration levels were 1300, 4000, 2200 ppmv, respectively. Fig. 6 shows the measured concentration results when the concentration level was increased from 1300 to 4000 ppmv and then was decreased to 2200 ppmv. Every gas sample was measured for ~ 5 min after the sensor reading was stable. During the test, the total flow rate of the sensor system was 130 mL/min. The MPGC has a volume of ~ 340 mL and was connected with the outlet of the gas mixing system by a pipe line with a volume of ~ 80 mL. Hence, the gas flow time was ~ 3 min. In addition, the gas preparation time of the mixing system to obtain a stable concentration should also be considered. According to the experimental results in Fig. 6, the rise time was measured to be ~ 290 s and fall time was ~ 200 s without excluding the gas mixing time.

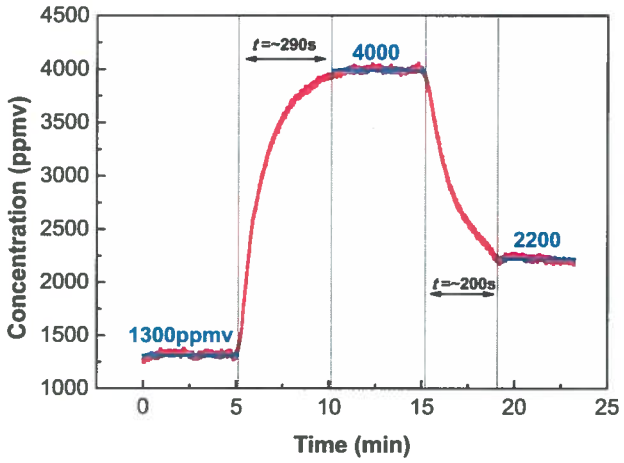


Figure 6. Response time measurements by switching gas samples with different concentration levels using the gas mixing system.

### 3.4 Deployment of the sensor system

Another four gas cylinders with a standard CO2 concentration level of 1500, 2500, 3500, 4500 ppmv were used to verify the detection performance and the linearity of the sensor system. Each gas sample was measured for ~ 5 min. For each group of measurement data, the averaged value was plotted versus the actual concentration of the sample with error bar as depicted in Fig. 7(a). The red line in the Fig. 7 (a) represented by $y = x$ indicates that the detection results of these gas samples had a good linearity.

A detection of human breath gas analysis was performed to observe the sensor behavior. An oil-free vacuum pump (KNF Neuberger Inc., Model N816.3KN.18) was employed to pump the human breath from the inlet of the MPGC. The response of the sensor system was recorded and exhibited in Fig. 7(b). Each peak represents a human breath. The two blue dash lines represent the maximum CO2 concentration and the minimum concentration, respectively. The CO2 concentration in the indoor atmosphere was ~ 400 ppmv according to the baseline of the data. The concentration of the breath CO2 gas was ~ 5.9%. Also, by analyzing the detailed data recorded during a concentration change, the rise and fall time were determined to be ~ 10 s excluding the gas mixing time.

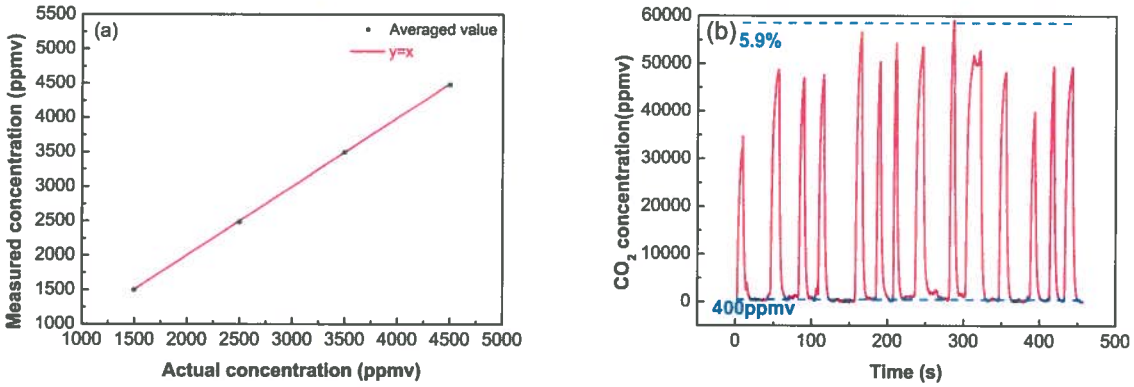


Figure 7. Deployment of the $CO_2$ sensor system. (a) Measured $CO_2$ concentration of four gas samples versus the theoretical concentration of 1500, 2500, 3500, 4500 ppmv. (b) Measured $CO_2$ concentration by pumping human breath gas into the cell.

## 4. CONCLUSIONS

We reported the development of a compact folded optical alignment structure, which can be employed in both near and mid-infrared gas detection based on TLAS. The established optical path is suitable for a sensor system using an MPGC without a fiber coupler for light injection. Based on this structure, a $CO_2$ sensor system consisting of a DFB laser, an IGA detector and a MPGC with a 29.8 m optical path length was developed. All the components of both the optical sub-system and the electrical sub-system were assembled into a standalone system for deployment. The DFB laser was operated to target a $CO_2$ absorption line located at 6359.96 $cm^{-1}$. Sensor calibration within a concentration range of 0 – 5000 ppmv was performed and a series of experiments were carried out to assess the performance of the system. Based on an Allan deviation analysis, a LoD of ~7.1 ppmv at a 0.4 s averaging time was obtained and at an optimum averaging time of 153.6 s, the LoD was reduced to ~ 277 ppbv. The rise and fall time at a dynamic operation were measured to be ~ 290 s and ~ 200 s, respectively, including the gas preparation time of the gas mixing system.

## ACKNOWLEDGEMENTS

The authors wish to express their gratitude to the National Key R&D Program of China (No. 2016YFC0303902), National Natural Science Foundation of China (Nos. 61775079, 61627823), Key Science and Technology R&D Program of Jilin Province, China (No. 20180201046GX), Science and Technology Planning Project of Guangdong Province, China (No. 2017A020216011), Industrial Innovation Program of Jilin Province, China (No. 2017C027), and National Science Foundation (NSF) ERC MIRTHE award and the Robert Welch Foundation (No. R4925U).

## REFERENCES


[1] Haq, B.U., "Methane in the Deep Blue Sea," Science 285, 543-544 (1999).

[2] Parlaktuna, M., Erdogmus, T., "Natural Gas Hydrate Potential of the Black Sea," Energy sources 23(3), 203-211 (2010).

[3] Ker, S., Le Gonidec, Y., Marsset, B., Westbrook, G.K., Gibert, D. and Minshull, T.A., "Fine-scale gas distribution in marine sediments assessed from deep-towed seismic data," Geophys. J. Int. 196(3), 1466-1470 (2014).

[4] Lu, W.J., Chou, I.M. and Burruss, R.C., "Determination of methane concentrations in water in equilibrium with sI methane hydrate in the absence of a vapor phase by in situ Raman spectroscopy," Geochim. Cosmochim. Ac. 72(2), 412–422 (2008).

[5] Song, F., Zheng, C.T., Yan, W.H., Ye W.L., Wang, Y.D. and Tittle F.K., "Interband cascade laser based mid-infrared methane sensor system using a novel electrical-domain self-adaptive direct laser absorption spectroscopy (SA-DLAS)," Opt. express 25(25), 31876-31888 (2017).

[6] Silver, J.A., "Frequency-modulation spectroscopy for trace species detection: theory and comparison among experimental methods," Appl. Opt. 31(6), 707–717 (1992).

[7] Werle, P., "A review of recent advances in semiconductor laser based gas monitors," Spectrochim. Acta. A 54(2), 197–236 (1998).

[8] Schilt, S., Thévenaz, L. and Robert, P. "Wavelength modulation spectroscopy: combined frequency and intensity laser modulation," Appl. Opt. 42(33), 6728–6738 (2003).

[9] Wysocki, G., Bakhirkin, Y., So, S., Tittel, F.K., Hill, C.J., Yang, R.Q. and Fraser, M.P., "Dual interband cascade laser based trace-gas sensor for environmental monitoring," Appl. Opt. 46(33), 8202–8210 (2007).

[10] Fiddler, M.N., Begashaw, I., Mickens, M.A., Collingwood, M.S., Assefa, Z. and Bililign, S., "Laser spectroscopy for atmospheric and environmental sensing," Sensors 9(12), 10447–10512 (2009).

[11] Curl, R.F., Capasso, F., Gmachl, C., Kosterev, A.A., McManus, B., Lewicki, R., Pusharsky, M., Wysocki, G. and Tittel, F.K., "Quantum cascade lasers in chemical physics," Chem. Phys. Lett. Front. Artic. 487(1-3), 1–18 (2010).

[12] Wysocki, G., Kosterev, A.A. and Tittel, F.K., "Spectroscopic trace-gas sensor with rapidly scanned wavelengths of a pulsed quantum cascade laser for in situ NO monitoring of industrial exhaust systems," Appl. Phys. B 80(4-5), 617–625 (2005).

[13] Lewander, M., Guan, Z.G., Persson, L., Olsson, A. and Svanberg, S., "Food monitoring based on diode laser gas spectroscopy," Appl. Phys. B 93(2-3), 619–625 (2008).

[14] Tranchart, S., Bachir, I.H. and Destombes, J.L., "Sensitive trace gas detection with near-infrared laser diodes and an integrating sphere," Appl. Opt. 35(36), 7070-4 (1996).

[15] Li, B., He, Q.X., Liu, H.F. and Wang, Y.D., "A trace gas sensor using near infrared distributed feedback laser at 1654nm," Laser physics 25(8), 086001 (2015).

[16] Li, C.G., Zheng, C.T., Dong, L., Ye, W.L., Tittel, F.K. and Wang, Y.D., "Ppb-level mid-infrared ethane detection based on three measurement schemes using a 3.34-μm continuous-wave interband cascade laser," Appl. Phys. B 122(7), 185 (2016).

[17] Li, C.G., Dong, L., Zheng, C.T. and Tittel, F.K., "Compact TDLAS based optical sensor for ppb-level ethane detectionby use of a 3.34μm room-temperature CW interband cascade laser," Sens. Actuators B Chem. 232, 188–194 (2016).

[18] Ye, W.L., Li, C.G., Zheng, C.T., Sanchez, N.P., Gluszek, A.K., Hudzikowski, A.J., Dong, L., Griffin, R.J. and Tittel, F.K., "Mid-infrared dual-gas sensor for simultaneous detection of methane and ethane using a single continuous-wave interband cascade laser," Opt. express 24(15), 16973-16985 (2016).

[19] Liu, K., Wang, L., Tan, T., Wang, G.S., Zhang, W.J., Chen, W.D. and Gao, X.M., "Highly sensitive detection of methane by near-infrared laser absorption spectroscopy using a compact dense-pattern multi-pass cell," Sens. Actuators B Chem. 220, 1000-1005 (2015).

[20] Daniel, O.B., Mark, E.P. and David, S.B., "Frequency modulation multiplexing for simultaneous detection of multiple gases by use of wavelength modulation spectroscopy with diode lasers," Appl. Opt. 37(12), 2499-2501 (1998).

[21] Cui, H.X., Du, Z.H., Chen, W.L., Qi, R.B. and Xu, K.X., "Applying diode laser wavelength modulation spectroscopy to detect oxygen concentration," Laser. Eng. 18(3-4), 263-270 (2008).

[22] Carpf, A. and Rao, G.N., "Absorption and wavelength modulation spectroscopy of NO2 using a tunable, external cavity continuous wave quantum cascade laser," Appl. Opt. 48(2), 408-413 (2009).
[23] Asakawa, T., Kanno, N. and Tonokura, K., "Diode Laser Detection of Greenhouse Gases in the Near-Infrared Region by Wavelength Modulation Spectroscopy: Pressure Dependence of the Detection Sensitivity," Sensors 10(5), 4686-4699 (2010).
[24] Gong, W., Ma, X., Han, G., Xiang, C.Z., Liang, A.L. and Fu, W.D., "Method for wavelength stabilization of pulsed difference frequency laser at 1572 nm for CO2 detection lidar," Opt. express 23(5), 6151-6170 (2015).